Acta Biomaterialia 77 (2018) 182–190

Contents lists available at ScienceDirect

Acta Biomaterialia

journal homepage: www.elsevier.com/locate/actabiomat

Full length article

Sortase A as a cross-linking enzyme in tissue engineering

Nicolas Broguiere, Florian A. Formica [1], Gonçalo Barreto [1], Marcy Zenobi-Wong *

Department of Health Science and Technology, ETH Zürich, Switzerland

ARTICLE INFO

Article history:
Received 20 February 2018
Received in revised form 24 June 2018
Accepted 9 July 2018
Available online 10 July 2018

Keywords:
Hydrogel
Cross-linking
Tissue engineering
Sortase

ABSTRACT

The bacterial ligase Sortase A (SA) and its mutated variants have become increasingly popular over the last years for post-translational protein modifications due to their unparalleled specificity and efficiency. The aim of this work was to study SA as a cross-linking enzyme for hydrogel-based tissue engineering. For this, we optimized SA pentamutant production and purification from *E. coli* to achieve high yields and purity. Then using hyaluronan (HA) as a model biopolymer and modifying it with SA-substrate peptides, we studied the cross-linking kinetics obtained with SA, the enzyme stability, cytocompatibility, and immunogenicity, and compared those to state-of-the-art standards. The transglutaminase activated factor XIII (FXIIIa) was used as the reference cross-linking enzyme, and the clinical collagen scaffold Chondro-Gide (CG) was used as a reference biocompatible material for in vivo studies. We found SA could be produced in large amounts in the lab without special equipment, whereas the only viable source of FXIIIa is currently a prescription medicine purified from donated blood. SA was also remarkably more stable in solution than FXIIIa, and it could provide even much faster gelation, making it possible to achieve nearly-instantaneous gel formation upon delivery with a double-barrel syringe. This is an interesting improvement for in vivo work, to allow in situ gel formation in a wet environment, and could also be useful for applications like bioprinting where very fast gelation is needed. The cytocompatibility and lack of immunogenicity were still uncompromised. These results support the use of SA as a versatile enzymatic cross-linking strategy for 3D culture and tissue engineering applications.

Statement of Significance

Enzymatic crosslinking has immense appeal for tissue engineers as one of the most biocompatible methods of hydrogel crosslinking. Sortase A has a number of unique advantages over previous systems. We show an impressive and tunable range of crosslinking kinetics, from almost instantaneous gelation to several minutes. We also demonstrate that Sortase A crosslinked hydrogels have good cytocompatibility and cause no immune reaction when implanted in vivo. With its additional benefits of excellent stability in solution and easy large-scale synthesis available to any lab, we believe this novel crosslinking modality will find multiple applications in high throughput screening, tissue engineering, and biofabrication.

1. Introduction

Hydrogels are widely used in the tissue engineering field for matrices supporting regeneration, as delivery vehicles for cells or pharmaceuticals, or for 3D culture applications. 3D cultures themselves have a range of applications from fundamental biology, e.g. trying to understand the interactions of cells with their matrix or studying the cell behavior in a more physiological environment, to practical uses such as drug screenings and creation of organs/tissues for transplantation [1–3].

While some polymers rely on non-covalent interactions for gel formation (e.g. collagen, self-assembling peptides, alginate, agarose), in most cases a bond-forming chemical reaction is needed to cross-link the gels. The choice of the cross-linking scheme is critical to the properties of the gels, as it directly influences the gelling kinetics, the cytocompatibility, stability in storage, the adhesion to tissue, and the biocompatibility in vivo. Bond forming reactions based on reactive chemicals typically make use of strong nucleophiles or electrophiles (e.g. Michael addition of thiols on maleimides/vinylsulfones/acrylates, Schiff-base formation from amines/hydroxylamines/hydrazides and aldehydes) which can

* Corresponding author.
E-mail address: marcy.zenobi@hest.ethz.ch (M. Zenobi-Wong).
[1] Equal contributions.

https://doi.org/10.1016/j.actbio.2018.07.020
1742-7061/

readily give side reactions with biological material (e.g. reaction with thiols or amines on proteins including on the cell surface [4], thiol-disulfide exchange reactions [5]). Another widespread chemistry for cross-linking is free-radical polymerization (e.g. Irgacure triggered photopolymerization of methacrylates, various implementations of thiol-ene addition), which is even less specific and can result in cell damage [6,7]. More recently, copper-free click chemistry provided much more specific chemical reactions, but at the expanse of large hydrophobic chemical groups (e.g. substituted cyclooctynes) which may readily physically intercalate with proteins resulting in non-specific binding [8–11]. All these common coupling methods with the advantages they can provide and some of their side-reactions and limitations have been reviewed recently [12].

In this context, enzymatic bond-forming reactions have become popular because of their good kinetics combined with excellent specificity [13]. The specific substrates of known bond-forming enzymes are typically peptides inspired from their natural targets and produced by solid phase supported synthesis. The transglutaminase activated factor XIII (FXIIIa), which is part of the blood coagulation cascade as a fibrin clot stabilizer, has found particularly widespread use in the research community because of its commercial availability in clinical quality and reasonably large quantities (clinical product Fibrogammin from CSL Behring), good kinetics, good specificity, and excellent biocompatibility in a wealth of applications. As a result, many biological or engineered building blocks have been modified chemically to display the peptides needed for coupling with FXIIIa, which created a convenient toolbox for the tissue engineering community [14–19]. In this cross-linking scheme, the polymers precursors are functionalized with peptides which are essentially inert from a chemical point of view, but which are recognized and ligated with an amide linkage in the presence of the enzyme. The most common strategy to conjugate the peptides to the molecules of interest (polymers or biomolecules) is to use peptides featuring a thiol group (on the side-chain of a cysteine residue, readily included during peptide synthesis) reacted on the receiving macromolecule featuring a Michael acceptor such as a vinylsulfone.

Even though FXIIIa shows excellent results as a cross-linking enzyme for hydrogel applications, a few things limit its applications. Firstly, FXIIIa is poorly stable in solution, which makes it essential to work with a freshly unfrozen aliquot or freshly resuspended powder, and any delay or freeze-thaw cycle is detrimental to reproducibility. Secondly, gelation speed reaches a plateau at FXIIIa concentrations higher than 20 U/ml, after which the speed increases only marginally when more enzyme is added. As a prescription medicine isolated from human blood, FXIIIa is also sometimes difficult for researchers to access, and it is in general ethically preferable to avoid resorting to material isolated from animals or human donors. Recombinant FXIIIa is also commercially available, however the price of these products is prohibitive, given quantities needed for bulk material science applications.

The bacterial ligase Sortase A (SA) has shown great promises in the field of drug-protein conjugation owing to its unparalleled kinetics and specificity [20], which motivated this evaluation of its potential as a cross-linking enzyme in the tissue engineering field. It has also been used to post-modify hydrogels [21], to dissolve hydrogels in mild conditions [22], and its orthogonality to mushroom tyrosinase has been recently exploited to make hydrogels stiffening over time [23]. To further evaluate the suitability of SA for hydrogel cross-linking in tissue engineering applications, we studied enzyme production, enzyme stability, hydrogel cross-linking kinetics, cytocompatibility, and in vivo biocompatibility. State-of-the-art scaffolds and enzymes were used as controls for comparison. The strategy employed for making biopolymers cross-linkable with SA is identical to the traditional methodology described above for FXIIIa cross-linking. Biopolymers are first functionalized with vinylsulfones, and then peptides harboring a thiol functional group are conjugated by Michael addition. In the presence of the enzyme, polymers featuring the two SA recognition motifs, namely LPXTGX and GGGG, are cross-linked into a gel, as illustrated in Fig. 1.

2. Materials and methods

Chemicals were purchased from Sigma and cell culture reagents from ThermoFisher/Invitrogen unless indicated otherwise.

2.1. Enzyme production

We used the plasmid including SA pentamutant (eSrtA) [24] in the expression vector pET29 kindly shared by Prof. David Liu through Addgene (#75144). Electrocompetent *E. coli* BL21(DE3) were transformed with the plasmid and a single colony with good protein expression was selected, expanded and frozen. For upscaled production, 12 ml LB-medium with 50 μg/ml kanamycin were inoculated and cultured at 37 °C, 180 rpm overnight. Then two flasks with 500 ml of this medium were inoculated with 5 ml of the overnight culture each and incubated at 37 °C, 180 rpm until OD_{600} = 0.8. This was typically reached after 3h30min. The protein production was then induced by addition of 0.2 mM IPTG and left

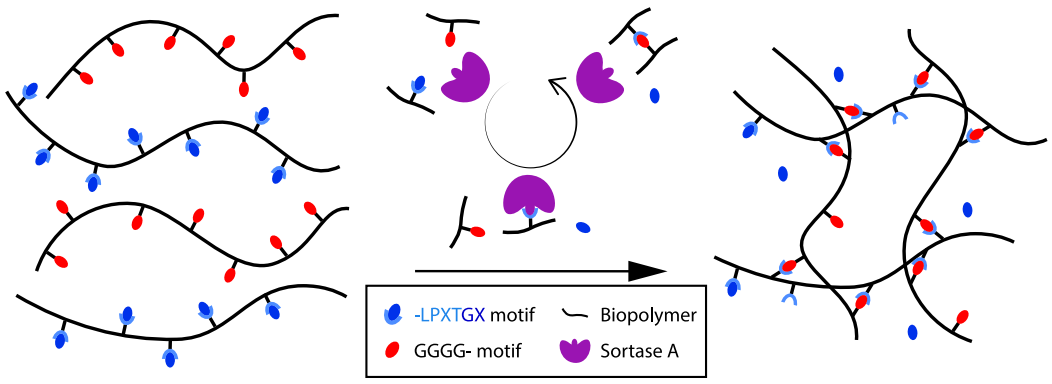

Fig. 1. Hydrogel cross-linking with Sortase A. The catalytic cycle, where the enzyme first removes the C-terminal GX of the LPXTGX peptide to form a thioester intermediate with -LPXT- and then gets attacked by the N-terminus of the GGGG- motif to form cross-links of sequence -LPXTGGGG- is represented in the middle. X represents any aminoacid (in this work: LPXTGX = LPETGG).

to proceed at 16 °C for 22 h. The bacteria were pelleted by centrifugation and resuspended in either BugBuster master mix (BB, Merck 71456) for surfactant-based lysis or tris buffered saline (TBS, 50 mM Tris, 150 mM NaCl, pH 7.5) supplemented with 10 mM imidazole, 1 mg/ml lysozyme and 1 mM β-mercaptoethanol (βM) for mechanical lysis. The two methods tested for mechanical lysis were sonication (three 10 s bursts at 50% intensity on a Digital Sonifier 250, Branson, Danbury CT, USA) and vortexing with Zirconium beads (ZB, OPS diagnostics PFAW 100-100-26), according to the manufacturer's instructions. The cells were pre-incubated for 30 min in the lysozyme containing buffer on ice before the mechanical treatment. The surfactant-based lysis was only left to proceed for 30 min at room temperature with gentle shaking. Finally, the cell debris were pelleted by centrifugation (20000*g* for 30 min at 4 °C) and the supernatant was collected for purification.

When comparing lysis methods, bacteria from the same culture were used in all conditions. In subsequent SA batches, only the surfactant-based lysis was used, and consistently gave similarly high yields.

2.2. Enzyme purification

The recovered lysate was filtered at 0.45 μm, and the SA was isolated using a His-Trap HP affinity column (GE Healthcare) mounted on a preparative HPLC (Agilent 1260 infinity). The eluent was TBS + 1 mM βM with 10 mM imidazole for 10 min, then a gradient from 10 to 250 mM imidazole over 30 min. The protein was re-concentrated at 4500 rcf and 4 °C with Vivaspin centrifugal filters, 10 kDa molecular weight cut-off (MWCO). Subsequently, the endotoxin level was reduced using Pierce high capacity endotoxin removal spin columns (Thermo) according to the manufacturer's protocol. Finally, the protein was dialyzed against TBS + 1 mM βM at 4 °C with a 1 kDa MWCO membrane, with 4 buffer changes over 6 h each.

The protein was diluted with an equal volume of TBS + 20% glycerol, and further diluted to adjust the concentration to 500 μM, using TBS + 10% glycerol. This final SA stock was filtered at 0.2 μm and stored at −80 °C in small aliquots.

The SA concentration was quantified at each step from the area under the peak at 280 nm on analytical gel permeation chromatography (GPC) with an Agilent Aquagel 20 column, 7.8 × 300 mm, with 5 μm particle size, using TBS 0.5 ml/min as the eluent. The concentration of the final purified product was also confirmed using the OD_{280} on a plate reader. We used the previously published value [33] of $\varepsilon_{280} = 17420\ M^{-1}\ cm^{-1}$, and albumin was used as a control of correct instrument calibration.

2.3. Endotoxin activity measurements

Endotoxin induced TLR4 activation was measured using a HEK-Blue hTLR4 assay according to the manufacturer's instructions (InvivoGen, San Diego, CA, USA). HEK-hTLR4 cells express TLR4 and MD-2/CD14 co-receptor genes of human origin and contain a secreted embryonic alkaline phosphatase (SEAP) reporter gene for monitoring NF-κB activation. Upon recognition of a ligand, TLR4 dimerizes and transduces a signal which results in NF-κB activation and SEAP secretion, which can be quantified with a colorimetric assay (QUANTI-Blue; InvivoGen).

Briefly HEK-Blue hTLR4 cells were seeded at 2.5×10^4 cells/well in 96-well microplates and maintained in Dulbecco's modified Eagle's medium (DMEM) with selective antibiotics, according to the manufacturer's protocol (InvivoGen). Cells were then stimulated for 24 h with a dilution series of SA or with purified LPS as a positive control (Invivogen tlrl-peklps). In parallel, the same conditions supplemented with CLI-095 (Invivogen, tlrl-cli95), a known TLR4 antagonist, were used to control the specificity of the effects. Finally, SEAP mediated change of QUANTI-blue in the conditioned culture medium was measured with a plate reader (Synergy H1).

2.4. HA-TG and HA-SA synthesis

A detailed protocol for the synthesis of HA-TG was described previously [18,19] with the FXIIIa substrate peptides Ac-FKGG-ERCG-NH_2 and NQEQVSPL-ERCG-NH_2. HA-SA was synthesized using the exact same protocol, except the peptides were the SA substrate peptides GGGG-LERCL-NH_2 and GCRE-LPETGG-NH_2 (Ac- refers to acetylated N-terminus, -NH2 refers to amidated C-terminus). In short, 10% of the carboxylate groups of HA are substituted with 3,3′-dithiobis(propanoic dihydrazide) (DTPHY) using EDC chemistry. The disulfides are then reduced to thiols, which are reacted with an excess of divinylsulfone to yield HA-vinylsulfone. Finally, the peptides are added by Michael addition. All purifications are done by dialysis. In this work, the HA substitution with vinylsulfones was confirmed by NMR, as well as disappearance of the vinylsulfone peaks upon peptide conjugation, and the substitution ratio of the final HA-peptide conjugate was found to be of 9.6% (Fig. S2).

Supplementary Figs. S1–S4 associated with this article can be found, in the online version, at https://doi.org/10.1016/j.actbio.2018.07.020.

The peptides were synthesized with classical fmoc solid phase supported peptide synthesis on rink amide resin and purified with C18 HPLC. The traditional cassette GCRE in the peptides is used for conjugation to vinylsulfonated HA by Michael addition, using the thiol functionality on the side chain of the cysteine. The positively charged arginine neighboring the cysteine favors deprotonation and increases the reactivity of this thiol, as shown by Lutolf et al. [34]. This cassette is modified to the more hydrophobic variant LERCL for the G_4 containing peptide in order to prevent this small hydrophilic sequence from eluting with the injection peak on HPLC, which facilitates its purification and analysis. Peptide purity was confirmed by high performance liquid chromatography (HPLC) on an Agilent 1260 infinity instrument, using a Poroshell EC-C18, 2.7 μm bead size, 4.6 × 100 mm column, with monitoring of the absorbance at 214 nm. Peptide identity was confirmed by electrospray ionization mass spectroscopy (ESI) on a Water instrument equipped with a single quadrupole detector SQ 2 (Fig. S1).

The HA substituted with the G_4 and LPXTG motifs were synthesized and stored separately, lyophilized at −20 °C, then resuspended in TBS and combined in equal amounts to form a 1.5% (w/v) mix stock solution.

2.5. PEG-SA synthesis

4-arm-PEG-vinylsulfone was formed by reacting 4-arm-PEG-thiol (20 kDa, LaysanBio) with 40 equivalents of divinylsulfone in triethanolamine buffer (300 mM, pH 8.0) for 30 min at room temperature, and purified by dialysis against ultrapure water, before lyophilizing for storage. Full conversion was confirmed by NMR.

4-arm-PEG-GGGG and 4-arm-PEG-LPXTG were formed by reacting 1.05 equivalents of the peptides GGGG-LERCL-NH_2 and GCRE-LPETGG-NH_2 (molarities of peptides stocks measured with the Ellman's assay) with 4-arm-PEG-vinylsulfone at 5% (w/v) for 1 h at 50 °C in triethanolamine buffer, 300 mM, pH 7.5. The resulting PEG-peptide conjugates were used without further purification.

For PEG-SA gel formation, the 5% stocks of 4-arm-PEG-GGG and 4-arm-PEG-LPXTG were mixed in equal quantities, and supplemented with SA 500 μM stock, $CaCl_2$ 100 mM stock, and TBS to achieve the concentrations reported (PEG 2%, SA 4-10-20 μM, $CaCl_2$ 10 mM).

2.6. Rheometry and gelation kinetics

Gelation was monitored on an Anton Paar MCR 301 rheometer equipped with a 20 mm plate–plate geometry and metal floor, pre-warmed to 37 °C and with a humidified chamber. The storage and loss moduli were monitored at 1 Hz with 4% strain and 20 s steps, after introducing between the two plates the hydrogel precursors swiftly mixed. The measurements shown are with the same mix used for the cytocompatibility and in vivo tests i.e. 1% (w/v), as well as 0.25 and 0.5% showing tunability of the stiffness.

Gelation using more than 2 μM of SA occurs too quickly for rheological monitoring, and the kinetics of gelation were therefore quantified manually. A timer was launched as the enzyme was added to the HA-SA stock (combined with TBS and $CaCl_2$ 100 mM stock for final concentrations of 1% (w/v) HA-SA and 10 mM $CaCl_2$), and the solution was pipetted slowly up and down until it suddenly sets into a gel which clogs the pipette, which was defined as the gelation time. The measurement was repeated three times for each condition. Gelation times for HA-SA were compared to that of HA-TG with varying amounts of FXIIIa (in TBS pH 7.6 and with 50 mM $CaCl_2$).

2.7. Enzyme stability

Enzyme stocks, tested for normal gelling kinetics upon fresh unfreezing, were tested again after 24 h at room temperature by testing the gelling time obtained with FXIIIa 20 U/ml and SA 2 μM. The remaining enzymatic activity was inferred from the gelation time obtained, using the gelation time vs activity curve previously constructed.

2.8. Microstructure imaging

HA-SA formed with 1% (w/v) polymer content and 2 μM SA was stained on amino groups with 1% (w/v) FITC in carbonate buffer, 100 mM, pH 9.5 for 1 h 30. The gel was then washed with PBS for 24 h with frequent buffer changes. The microstructured was imaged on a Leica SP8 microscope with a 64× Oil objective, and deconvolved with Huygens with a point spread function estimated from the imaging parameters using the Leica-Huygens link.

HA-TG was formed with 1% (w/v) polymer content and 20 U/ml FXIIIa in the presence of 200 μM of a fluorescein tagged NQEQVSPLERCG-NH2 peptide. The resulting gel was washed with TBS and PBS and imaged in the same conditions.

The tagged peptide was formed by reacting 1 equivalent of fluorescein-5-maleimide (Thermo) with 10 mg of NQEQVSPLERCG-NH2 (purchased from Anawa) for 5 min in 2 ml of triethanolamine buffer (150 mM, pH8.0) followed by hydrolysis of the maleimide ring to prevent retro-Michael addition by treatment with NaOH pH 10 overnight. The conjugation and hydrolysis were monitored by HPLC. The product was purified by dialysis against ultrapure water, and the identity of the final peptide-fluorescein conjugate was confirmed by matrix assisted laser desorption and ionization mass spectrometry (MALDI). Expected molecular mass (with hydrolyzed maleimide ring and one proton): 1805.99. Mass found: 1805.918.

2.9. Cytocompatibility with cell encapsulation

Human chondroprogenitor cells (hCC) were cultured as described previously [18]. For encapsulation, the cells were pelleted and resuspended at 5e6 cells/ml in TBS with 1% (w/v) HA-SA, 10 mM $CaCl_2$ and 2 μm SA from concentrated stocks. The precursor mix was cast in 4 mm diameter PDMS rings adhered on coverslips. Cross-linking was left to proceed for 8 min before covering with DMEM + 10% FBS. The viability before encapsulation was measured by trypan blue exclusion on a Countess device (Thermo). The viability 24 h after encapsulation was measured with calcein-AM (live cells cytoplasm green), Hoechst (all cells nuclei blue) and propidium iodide (PI, dead cells nuclei red), imaged with a Zeiss observer widefield microscope on two volumes of $1.4 \times 1 \times 0.1$ mm^3 in each gel on 4 independent gels, followed by manual counting in Image J. The viability 12 days after encapsulation was measured from calcein-AM and Hoechst imaged on a Leica SP8 multiphoton microscope.

2.10. MTS assay

Human embryonic kidney cells were seeded at 10,000 cells/cm^2 in a 24-well plate. In the positive control, the cells were cultured with 500 μl of DMEM + 10% fetal bovine serum (FBS) per well for 4 days. In the vehicle control, 10% of the medium was replaced by TBS for the whole culture period. In the HA-SA conditions, 10% of the medium was replaced with 1.5% HA-GGGG or 1.5% HA-LPXTG stocks in TBS, and 4 μM of SA from the 500 μM stock were added, also kept for the whole culture period. For the final MTS assay (abcam), the medium was replaced by phenol-red free DMEM supplemented with 10% of the commercial MTS reagent solution, before returning the plate to the incubator for 1 h, and finally measuring the absorbance on a plate reader.

Statistical analysis was done with one-way ANOVA with Matlab (ANOVA p value 2.2e-9) with Tukey's post-hoc testing.

2.11. Subcutaneous implantations

In vivo trials were approved by the Zürich Veterinary Office and performed according to animal welfare regulations and guidelines (License ZH189/2014). Cell-free HA-SA gels (1% (w/v) with 2 μM SA) of 8 mm diameter × 1.5 mm height and control patches of the clinical collagen scaffolds CG of the same dimensions were implanted in subcutaneous pockets of female C57BL/6 mice. Analgesia with 2 mg/kg subcutaneous Metacam was provided 30 min before surgery. Isoflurane was used for anesthesia. The experiments included three animals per condition, with two lumbar implantation sites per animal, for a total of 6 scaffolds per condition. The animals were monitored daily for 7 days, and no occurrence of weight loss, redness or swelling was found. Sacrifice was performed two weeks after implantation and at this time, blood for analysis of inflammatory markers was collected by cardiac puncture.

2.12. Serum inflammation marker measurements

Mouse blood serum was prepared by clotting the whole blood (≈150–300 μl) for 30 min at RT followed by centrifugation at 10,000 rpm for 10 min at RT. The supernatant was then collected and frozen at −80 °C until further analysis.

The serum concentrations of the interleukins IL-1β, IL-4, IL-6, and IL-10 as well as the cytokine TNF-α were quantified with the multiplex immunoassay technology xMAP on a MAGPIX instrument (Luminex, Austin, TX, USA), according to manufacturer's instructions. The mouse serum was diluted 1:3 in the serum compatible "Universal Assay Buffer", and the measurements were performed with a custom designed multiplex assay kit (IL-1β – EPX01A-26002-901; IL-4 – EPX01A-20613-901; IL-6 – EPX01A-20603-901; IL-10 – EPX01A-20614-901; TNF-α – EPX01A-20607-901, ProcartaPlex assays; ThermoFisher). Protein levels were measured in technical duplicate for each of the 6 animals from 100 μl of the diluted serum. The calibration was performed using a serial dilution of the standard mix provided with the multiplex kit. The data was then fitted using a four-parameter logistic regression model. The quantification of the lower limit of detection (LOD) using this system was 2.7, 0.6, 0.6, 1.8 and 4.8 pg/ml for IL-10, IL-1β, IL-4, IL-6 and TNFα, respectively.

2.13. Immunohistochemistry

The scaffolds were explanted after two weeks, when possible together with the overlying skin tissue. They were fixed overnight with 10% formalin in PBS, and then incubated for 2 days in 30% sucrose. They were then transferred in Tissue-Tek optimal cutting temperature compound and frozen on dry ice. Cryosections at 50 µm thickness were collected. The sections were permeabilized with 0.3% triton-X 100 in TBS for 30 min, then blocked with 5% goat serum + 1% BSA for 1 h. Rabbit polyclonal anti CD-68 antibody (ab125212) was incubated at 1:200 in blocking solution overnight at room temperature, washed three times with TBS, and an HRP conjugated goat anti-rabbit secondary (ab6721) was used at 1:500 for 2 h at RT. 3,3′-Diaminobenzidine (DAB) with DAB enhancer (abcam) was used as a chromogen. The samples were counterstained with Hematoxylin (Richard-Allan, 3 min. Destain EtOH: H_2O:HCl 28:12:0.12 1 min. Blued 0.1% Na_2CO_3 1 min) and mounted with Eukitt quick hardening mounting medium. Imaging was done on a Zeiss Observer with a 5x tile-scan (overview) and a 10x extended focus scan (close-ups).

3. Results and discussion

3.1. Enzyme production

The SA pentamutant [24] (kindly shared by Chen Dorr and Liu on Addgene) was used due to its improved catalytic activity compared to the wild type SA. Purified protein yields of 40 mg/l of bacterial culture have been reported previously using French press lysis [20], which is an expensive equipment and needs experience to operate efficiently. Instead, we investigated traditional sonication (SN), lysis by vortexing with zirconium beads (ZB), and chemical lysis with a commercial mix of surfactants and enzymes (BugBuster, BB), and the combination of BB + ZB. In all cases, the crude bacterial extracts already consisted primarily of SA (Fig. 2A), but after purification using the His-tag and a nickel column, BB based conditions clearly stood out with yields of around 160 mg of purified SA per liter of bacterial culture (Fig. 2B). Combination of ZB with BB reduced the yield (probably by damaging proteins with heat and friction) rather than increasing it. It is particularly interesting that the BB method does not require any dedicated instrumentation and is fast and easy to handle even with no prior experience, making the SA production in high yields available to any lab.

One new concern that arises with the SA compared to FXIIIa is that bacterial production leaves endotoxin contamination in the protein, which can trigger inflammation or alter cell behavior. We confirmed that protein produced with no endotoxin removal step (SA-NER) contained enough endotoxins to trigger a plateau in the activity of NF-κB in TLR4 expressing HEK cells at every dilution tested from 50 to 4050 fold (Fig. 2C). We therefore post-purified the protein with endotoxin removal resin. The recovered protein (SA) still contained some endotoxin, but at a stock dilution of 450 (1.1 µM, close to the 2 µM used in most applications) the level of TLR4 activation was found to correspond to a purified lipopolysaccharide (LPS) content of around 0.5 ng/ml, which in endotoxin units (EU) corresponds to 0.5 EU/ml for the LPS strain we used. Since the US Food and Drug Administration (FDA) sets the limit to 0.5 EU/ml in eluates from medical devices soaked for 1 h in endotoxin-free water [25], the endotoxin content we obtained in our gels would satisfy FDA requirements (the concentrations in eluates from the gel can only be lower than the initial concentration in the gel itself). For particularly sensitive applications such as 3D cultures of immune cells, the post-purification could be repeated to further reduce the endotoxin level.

3.2. Hydrogel formation

Gelation speed can be particularly important for in vivo or clinical usage of a hydrogel/sealant/glue. When the gels must cross-link in a wet environment, such as in the presence of bleeding or in a fluid filled cavity, near instantaneous gelation is a strong

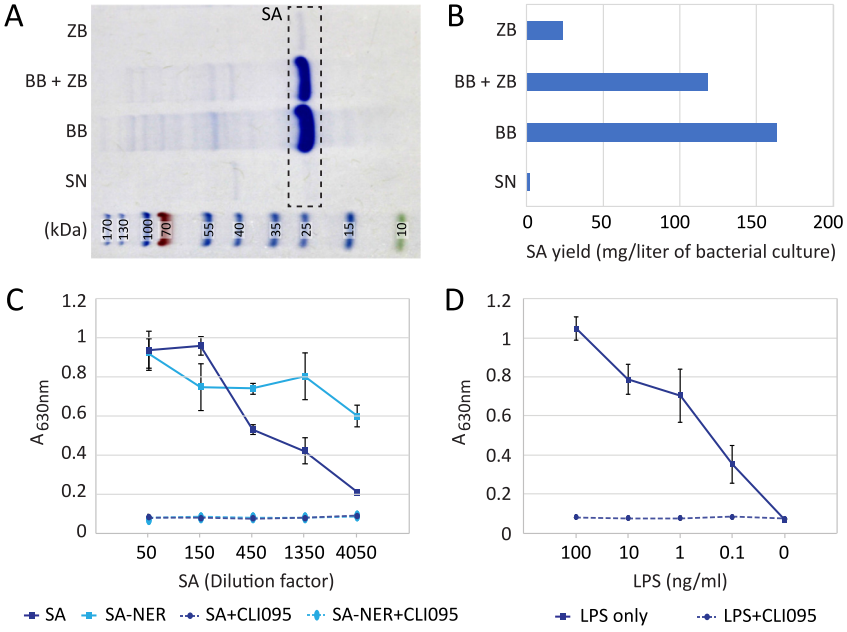

Fig. 2. Enzyme production. (A) SDS-PAGE comparison of the content of the crude extracts obtained with different lysis methods: vortexing with zirconium beads (ZB), treatment with BugBuster surfactant and enzyme mixture (BB), and sonication (SN). (B) Quantification by gel permeation chromatography (GPC) of the yields of SA obtained after His-tag purification. (C–D) Measurements of endotoxin activity with cells expressing the endotoxin-sensitive receptor TLR4, and a colorimetric reporter for its downstream target NF-κB. (C) Results obtained with serial dilutions of the 500 µM SA stock as well as an equivalent stock with no endotoxin removal step (SA-NER). CLI-095 is a selective TLR4 antagonist used in control experiments to ensure the specificity of the response. (D) Standard curve for purified LPS. Error bars: SD n = 3.

advantage. Fast gelation, traditionally of alginate in the presence of calcium or from thermo-responsive gels, has also been exploited in various implementations of bioprinting. The possibility to tune the gelation speed to around 30 s, which was already offered by transglutaminase cross-linkable hyaluronan and FXIIIa, is also ideal for 3D cell culture applications, since this is the best time to enable easy handling and casting but prevent cell sedimentation.

We therefore studied the gelation kinetics for HA gels cross-linked with SA, denoted HA-SA (which includes the two components HA-LPXTG and HA-GGGG) and compared them with the kinetics of FXIIIa cross-linked HA gels, denoted HA-TG, used as a state-of-the-art reference (Fig. 3A). The maximum enzyme concentrations tested were limited by the concentration of the stock solutions. Interestingly, we found that gelation speed with FXIIIa reached a plateau of ≈30 s, corresponding to ≈20–30 U/ml FXIIIa. Such saturation does not occur with SA which shows linear kinetics (i.e. doubling the amount of enzyme halves the gelation time) up until a gelation time lower than one second. This enables gelation to be performed in challenging environments with instant setting after injection from a double-barrel syringe. We demonstrated it by forming 0.75% gels directly under water (Fig. 3F).

Enzyme stability is also an interesting property, enabling better reproducibility and easier handling, which is ultimately also associated with lower costs in a clinical setup. Stability in solution is also essential for high content screening applications where the stock solutions are loaded in spotting robots which then work autonomously. It was therefore a great surprise to find that unlike FXIIIa, which loses roughly half of its activity over 24 h, SA could be kept in solution at room temperature without any loss of activity (Fig. 3B).

We also monitored the gelation of HA-SA on a rheometer using the same concentrations of polymer and enzyme as used for gel casting (i.e. 1% (w/v) HA-SA, 10 mM $CaCl_2$, 2 μM SA, in tris buffered saline (TBS) pH 7.5 which conveniently sets in ≈30 s). The overall gelation profile was remarkably reproducible (Fig. 3C), and looked similar to what is generally obtained with other cross-linking methods. The stiffness reached after completion of the cross-linking, approximately 100 Pa (115 ± 9, SD n = 4), is typical for hydrogels for 3D cell culture applications, and is in particular in the same range as other gels used for cell cultures [26] such as fibrin (3–6 mg/ml, 100–200 Pa), Matrigel (≈100 Pa), collagen gels (≈200 Pa), or soft polyethylene glycol (PEG) gels (100–500 Pa, e.g. [27]). 70% of the final stiffness was reached after 8 min, which gives a good indication of the time that the gels might be left to cross-link before transferring 3D cultures to medium. The strain and frequency response of 1% HA-SA gels were measured as well (Fig. S3) and confirmed the parameters used for gel monitoring are well within the linear viscoelastic range of the material. We also verified the classical result that changes in macromer concentration enables tuning of the mechanical properties: rheometry for gels containing 0.25% (close to the lowest stable hydrogels, similar to the situation with HA-TG [19]) and 0.5% macromer (soft gels typically used for neuronal cells [19]) are shown in Fig. 3C.

Due to the very high molecular weight of the HA used (1.6 MDa), hydrogels with macromer concentrations higher than 1% (w/v) were too viscous to be handled easily, and were not demonstrated. It is a classical result that high molecular weight polymer are geared towards low polymer content and low stiffness hydrogels, and not a particularity of the cross-linking scheme.

In order to validate that the cross-linking results were not a particularity linked to the use of HA as a model polymer, we also demonstrated gel formation from 4-arm-polyethylene glycol (PEG) hydrogels, end-functionalized with the LPXTG and GGGG motifs. Rheological measurements (Fig. 3D), for the 2% (w/v) PEG content (≈200 Pa) typically used for cell culture applications, showed that fast gelation with small amounts of SA, and tuning of the gelation time with SA concentration, could also be achieved. The concentration of SA needed for a given gelling time was nevertheless higher for PEG gels (roughly 10×, with 30 s gelling achieved at SA ≈20 μM), which is expected given the low molecular weight (20 kDa) of the polymer and the low number of functional groups (4) per building block compared to the HA gels.

It is noteworthy that in the only previous report of SA-mediated hydrogel cross-linking [23] that exists to our knowledge, enzyme

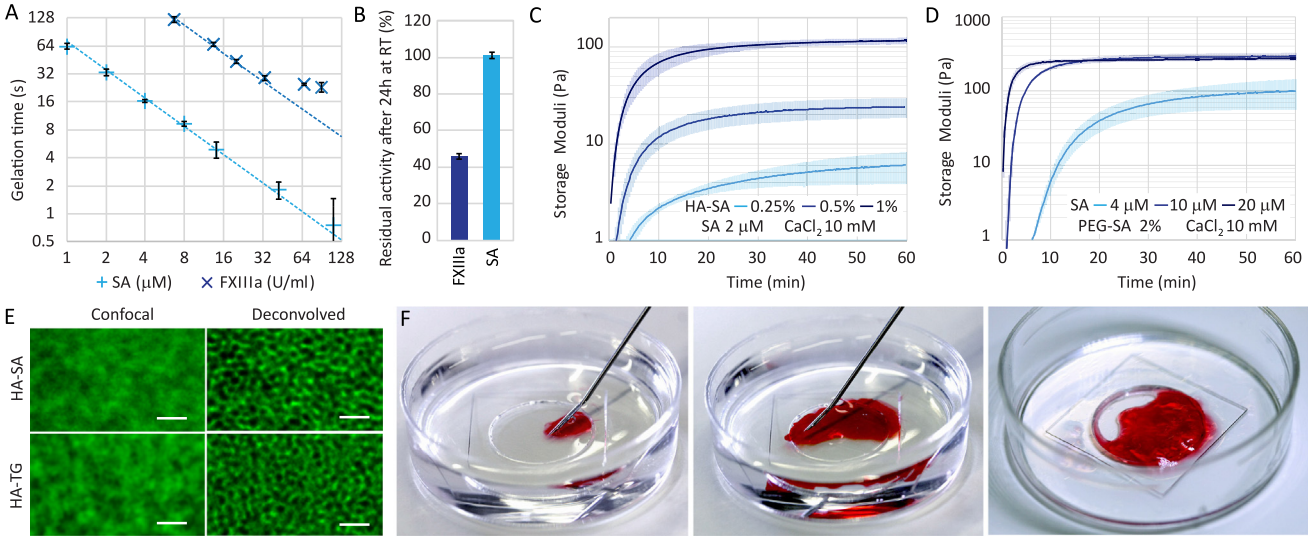

Fig. 3. Gelation kinetics and enzyme stability. (A) Manual measurements of gelation time of HA-SA 1% and HA-TG 1% with varying concentrations of SA and FXIIIa. Dotted lines are fits with inverse functions in the linear catalysis range of both enzymes. Error bars: SD n = 3. (B) Residual enzymatic activity after storage of enzyme stock solution for 24 h at room temperature, inferred from gelation time measurements and shown as a percentage of the activity in fresh stocks. Error bars: SD n = 3. (C) Gelation of HA-SA at various macromer content as monitored on a rheometer, showing the gelling profiles and stiffness tuning. Error bars: SD n = 4 (1%) and n = 3 (0.25 and 0.5%). (D) Demonstration of SA cross-linking on a polyethylene glycol (PEG) backbone with various SA concentrations, as monitored by rheometry. Error bars: SD n = 2. (E) Confocal fluorescence microscopy of the microstructures of HA 1% gels cross-linked with 2 mM SA and 20 U/ml FXIIIa respectively. Deconvolved images were obtained with Huygens. (F) Demonstration of underwater instant gelling after injection from a double barrel syringe with 1.5% HA-SA in one compartment and 250 μM SA + 20 mM $CaCl_2$ in the other, as well as phenol red for gel visualization. From left to right: beginning of injection, end of injection, and after removing the water.

concentrations needed to be orders of magnitude higher (600 μM for gelation in 90 s) than what is used in the protein field (around 10 μM), which seemed to be a major limitation. One difference in this previous work is that the LPXTG peptides used did not include an additional N-terminal glycine, but we found that this was not inducing any difference in our system (Fig. S4) and could not explain the differences of kinetics obtained. Enzyme concentrations of several hundred micromolars would make it nearly impossible to upscale the SA cross-linking system or target in vivo applications, we nevertheless show that cross-linking can be made very efficient, which is opening a completely different array of possibilities.

Finally, the microstructure of HA-TG 1% and HA-SA 1% was estimated using fluorescein-tagged hydrogels and confocal microscopy. A mesh with a typical size of ≈200 nm could be distinguished in both cases, with a very similar morphology. The resolution limit of light microscopy is a major limitation to the quality of the data in this case, but sample preparation for electron microscopy (EM) or cryo-EM would need dehydration or freezing, which could affect the positioning of these flexible hydrophilic soluble polymer chains more dramatically. Overall, the microstructure of the hydrogels does not seem to be affected by the difference in cross-linking chemistry, as is expected since both enzymes create step-growth polymerization with a very similar mechanism.

3.3. Cytocompatibility

Since human chondroprogenitor cells (hCCs) were already shown to thrive in HA gels [18], we chose to use them to test the cytocompatibility of HA-SA, reasoning that any loss of viability would be due to the change in cross-linking chemistry. We measured the viability 24 h and 12 days after encapsulation. Representative images (maximum intensity projections) are shown in Fig. 4A. We found the viabilities one day and 12 days post-encapsulation to be similar to the viability before encapsulation, all slightly above 90% (Fig. 4D).

These 3D cell cultures were also used to test if the HA-SA hydrogels retained sensitivity to hyaluronidase (HAse) degradation. We found that upon treatment with 1 mg/ml HAse in PBS for 2 h, the gels were entirely degraded. The cells which are initially scattered as single cells collapsed into loose cell aggregates upon treatment (Fig. 4B).

The 3D cultures are not the best situation to distinguish small effects on cell proliferation or metabolic activity, because cells might switch to a non-proliferative or low-proliferative state in 3D cultures, and subtle changes in physical properties of the scaffolds can have major effects on the cell proliferation. We therefore conducted an additional cytotoxicity assay using fast-proliferating human embryonic kidney (HEK) cells in 2D culture. The cells were seeded at very low density and left to proliferate for 4 days in the presence of HA-LPTXG or HA-GGGG as well as 4 μM SA. The cells were around 75% confluent at the end of the proliferation time, and their metabolic activity (which reflects cell number x cell health) was then measured with an MTS assay (Fig. 4C). We found that the cells cultured in the presence of HA-peptide derivatives and SA had the same vitality as the cells grown in the medium + delivery vehicle (10% TBS).

3.4. Biocompatibility in vivo

We had particular concerns about immunogenicity, since SA is a bacterial enzyme and produced in bacteria. We therefore checked for adverse reactions to SA in typical usage concentrations by implanting in mice subcutaneous cell-free HA-SA scaffolds of 8 mm diameter freshly formed with 2 μM SA. The collagen scaffold Chondro-Gide (CG), which is a clinical product, was used as a reference. We assessed the intensity of the foreign body response, which describes the non-specific immune response to implanted foreign materials, two weeks after subcutaneous implantation.

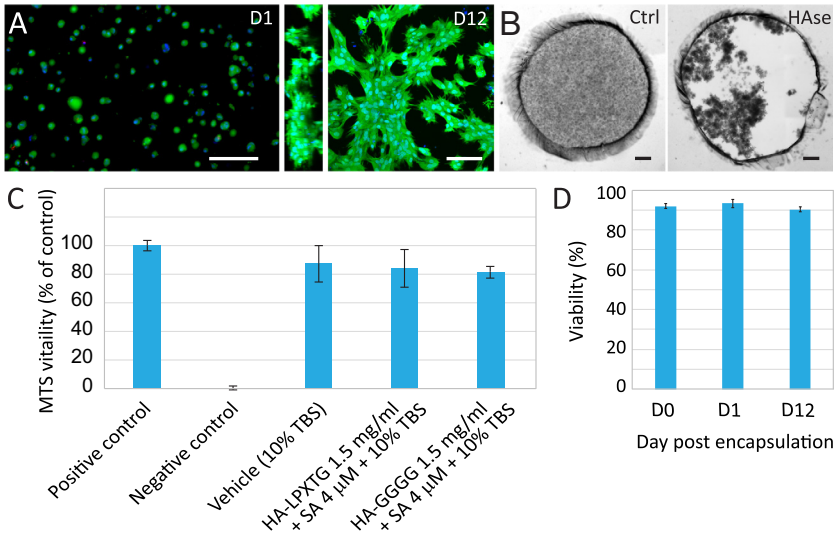

Fig. 4. Cytocompatibility of HA-SA. (A) Calcein/propidium iodide/Hoechst staining of human chondroprogenitor cells (hCCs) 24 h after encapsulation (D1) as seen in widefield fluorescence microscopy and calcein/Hoechst staining of hCCs 12 days after encapsulation (D12) as seen in two-photon microscopy, side and top view, maximum intensity projections over 50 μm. Scale bars: 100 μm. (B) Demonstration of HA-SA gel degradation upon treatment with hyaluronidase (HAse) 1 mg/ml in PBS for 2 h. An untreated control is shown as reference. The gels contain encapsulated hCCs, which are initially well dispersed but collapse into a dense aggregate upon gel removal. The surrounding structure is a PDMS cast. Scale bars: 500 μm. (C) Analysis of cytotoxicity using a colorimetric metabolic activity assay on human embryonic kidney (HEK) cells cultured over 4 days in 2D from low density to 70% confluence in the presence of the HA-SA gel components and controls. Both proliferation and metabolic activity need to be unaffected to reach the activity level of positive controls. Cells treated with 70% ethanol before the assay are used as a negative control, and all data is normalized to the controls (positive = 100% negative = 0%). There is no significant difference between the HA-SA components and the vehicle used to introduce them ($p = 0.98–0.99$). (D) Quantifications of the hCC viability before encapsulation (D0), and 1 and 12 days after encapsulation (D1, D12). SD n = 4.

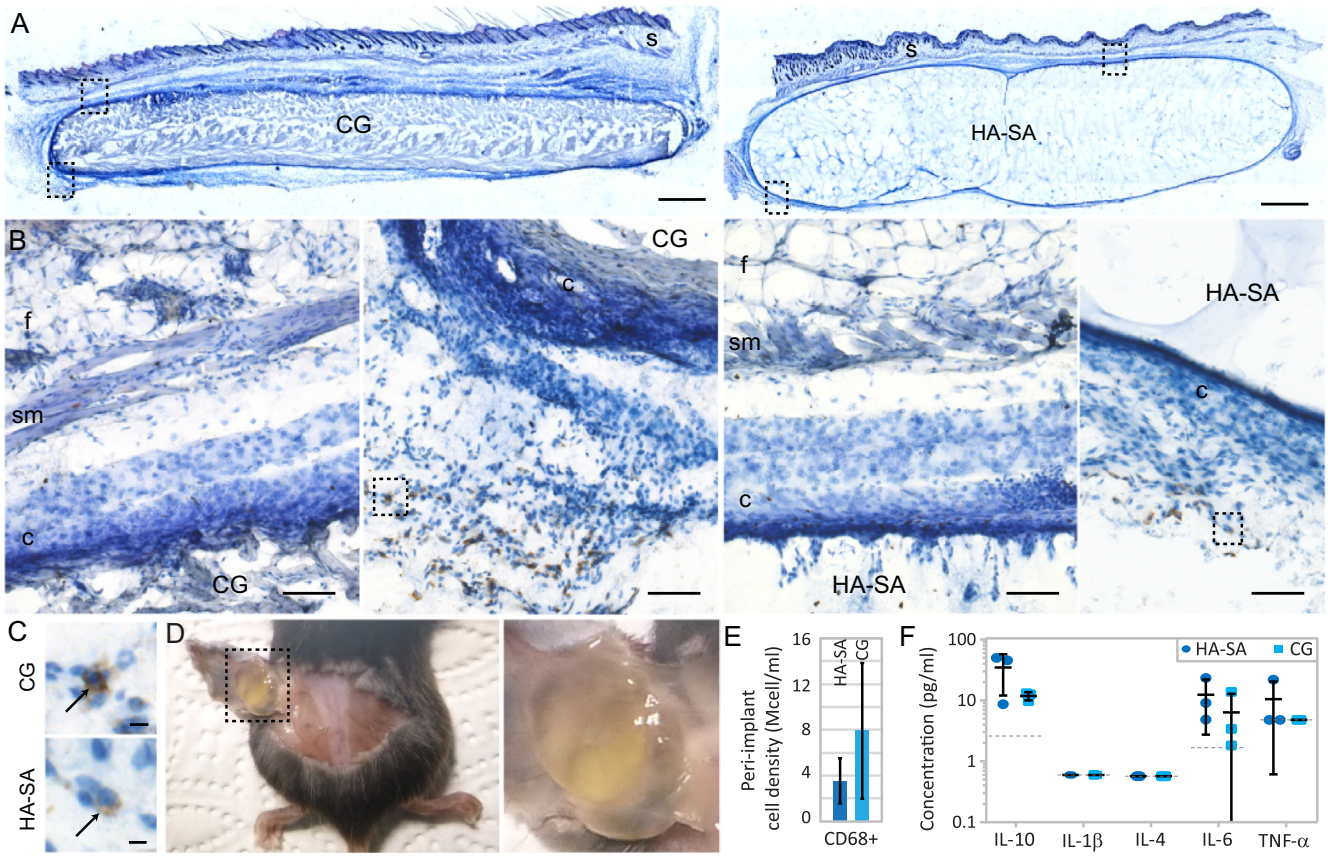

Fig. 5. Biocompatibility of HA-SA in vivo. (A) Cryosections of cell free sortase cross-linked hyaluronan (HA-SA) scaffolds and control clinical scaffolds chondrogide (CG) explanted 2 weeks after subcutaneous implantation in C57BL/6 mice, stained for nuclei (hematoxylin, blue) and the macrophage marker CD68 (DAB, brown). Scale bars: 1 mm. (B) Close-ups on the skin and body sides of the capsule from positions highlighted in A. Scale bars: 100 μm. Labels are skin (s) fat tissue (f) striated muscle from the panniculus carnosus (sm) and capsule (c). (C) Close-ups on typical CD68+ cells in the peri-scaffold tissue from positions highlighted in B. Scale bars: 10 μm. (D) HA-SA scaffolds upon recovery after two-weeks in vivo. The gels remained transparent and no macroscopic encapsulation or gel degradation is visible. (E) Quantification of the CD68 + macrophage density in the surroundings of the explanted scaffolds. CG is used as a reference. Error bars: SD n = 3 animals (with the counts from 8 fields of view around 2 scaffolds taken as a single average value for each animal). (F) Quantification of chronic inflammation markers in the serum of the mice 2 weeks after implantation. Dotted lines: limit of detection. Undetected cytokines are represented on the limit of detection. Error bars: SD n = 3 animals × 2 technical replicates. (For interpretation of the references to colour in this figure legend, the reader is referred to the web version of this article.)

In the general development of the response, the initial acute phase is resolved a few days after implantation [28]. It was therefore not studied at our timepoint.

In a second stage, one to three weeks after implantation, chronic inflammatory response follows [29]. The latter is associated with macrophage recruitment [30] and inflammatory cytokine secretion. We therefore quantified recruitment of CD68+ macrophages to the periphery of the implanted scaffolds, and found comparable cell densities around the HA-SA and CG reference (Fig. 5A–E). Upon recruitment, macrophages may polarize to an M1 "activated" phenotype depending on the pyrogen content (e.g. endotoxins) as well as the material's chemical, biophysical and mechanical properties. Once in M1 phenotype, macrophages secrete pro-inflammatory cytokines such IL-1β, IL-6 and TNFα which contribute to the recruitment of more macrophages. Using a multiplex assay to quantify the serum levels of various chronic inflammatory cytokines in the serum, we found that the levels of IL-1β, IL-6 and TNFα in the HA-SA group were comparable to the CG reference group (Fig. 5F). Extensive characterization and validation of this multiplexed assay for the analysis of serum cytokines has been done in previous studies, and cytokine levels in a variety of control and inflammatory conditions have been reported as well [31,32]. Interestingly, the values we obtained in both groups were similar to previously reported values in animals either untreated or implanted with a control saline-injecting mini-pump. Overall, the low systemic pro-inflammatory secretion levels by M1 macrophages and other immune cells, seem to indicate the materials are well tolerated.

Upon resolution of the chronic inflammatory response, a granulation phase follows, where typically macrophages switch polarization to the M2 phenotype and secrete anti-inflammatory molecules such as IL-4 and IL-10 which aid in the recruitment of tissue repair cells e.g. fibroblasts. We also found low levels of IL-4 and IL-10 in both groups, which is expected given the earlier timepoint studied.

4. Conclusion

In summary, we have found that SA fulfilled all the conditions to be an excellent cross-linking enzyme for tissue engineering applications. It provides unmatched kinetics for hydrogel formation, good enzyme stability, and can be produced in large amounts in the lab without any special equipment or training. Most importantly, it is also cytocompatible and does not trigger an adverse inflammatory reaction in vivo. These properties make SA cross-linked hydrogels attractive for a wide range of applications including large scale 3D screening platforms, bioprinting and in situ cross-linking in challenging surgical environments.

Acknowledgements

We would like to thank Prof. Lee Ann Applegate for providing the hCC cell line and David Fercher for technical assistance with bacterial cultures and protein production. We acknowledge funding from the Swiss National Science Foundation (grant no. CR32I3_166052 to MZW).

Disclosures

The authors have no competing interests to declare.

References

[1] E. Caló, V.V. Khutoryanskiy, Biomedical applications of hydrogels: a review of patents and commercial products, Eur. Polym. J. 65 (2015) 252–267.
[2] A.S. Hoffman, Hydrogels for biomedical applications, Adv. Drug Deliv. Rev. 64 (2012) 18–23.
[3] D. Seliktar, Designing cell-compatible hydrogels for biomedical applications, Science (80-) 336 (6085) (2012) 1124–1128.
[4] G. MacBeath, S.L. Schreiber, Printing proteins as microarrays for high-throughput function determination, Science (80-) 289 (2000) 1760–1763.
[5] H.F. Gilbert, Molecular and cellular aspects of thiol-disulfide exchange, Adv. Enzymol. Relat. Areas Mol. Biol. 63 (1963) 69–169.
[6] S.J. Stohs, The role of free radicals in toxicity and disease, J. Basic Clin. Physiol. Pharmacol. 6 (3–4) (1995) 205–228.
[7] S.J. Bryant, C.R. Nuttelman, K.S. Anseth, Cytocompatibility of UV and visible light photoinitiating systems on cultured NIH/3T3 fibroblasts in vitro, J. Biomater. Sci. Polym. Ed. 11 (5) (Jan. 2000) 439–457.
[8] J. Dommerholt et al., Readily accessible bicyclononynes for bioorthogonal labeling and three-dimensional imaging of living cells, Angew. Chem. Int. Ed. 49 (49) (2010) 9422–9425.
[9] M.F. Debets, S.S. Van Berkel, J. Dommerholt, A.J. Dirks, F.P.J.T. Rutjes, F.L. Van Delft, Bioconjugation with strained alkenes and alkynes, Acc. Chem. Res. 44 (9) (2011) 805–815.
[10] C. Freidel, S. Kaloyanova, K. Peneva, Chemical tags for site-specific fluorescent labeling of biomolecules, Amino Acids 48 (6) (2016) 1357–1372.
[11] E. Ostuni, R.G. Chapman, R.E. Holmlin, S. Takayama, G.M. Whitesides, A survey of structure-property relationships of surfaces that resist the adsorption of protein, Langmuir 17 (18) (2001) 5605–5620.
[12] S.A. Fisher, A.E.G. Baker, M.S. Shoichet, Designing peptide and protein modified hydrogels: selecting the optimal conjugation strategy, J. Am. Chem. Soc. 139 (22) (2017) 7416–7427.
[13] L.S.M. Teixeira, J. Feijen, C.A. van Blitterswijk, P.J. Dijkstra, M. Karperien, Enzyme-catalyzed crosslinkable hydrogels: emerging strategies for tissue engineering, Biomaterials 33 (5) (Mar. 2012) 1281–1290.
[14] F. Anjum, P.S. Lienemann, S. Metzger, J. Biernaskie, M.S. Kallos, M. Ehrbar, Enzyme responsive GAG-based natural-synthetic hybrid hydrogel for tunable growth factor delivery and stem cell differentiation, Biomaterials 87 (2016) 104–117.
[15] P.S. Lienemann et al., A versatile approach to engineering biomolecule-presenting cellular microenvironments, Adv. Healthc. Mater. 2 (2) (2013) 292–296.
[16] S. Metzger et al., Modular poly(ethylene glycol) matrices for the controlled 3D-localized osteogenic differentiation of mesenchymal stem cells, Adv. Healthc. Mater. 4 (4) (2015) 550–558.
[17] M. Ehrbar et al., Enzymatic formation of modular cell-instructive fibrin analogs for tissue engineering, Biomaterials 28 (26) (Sep. 2007) 3856–3866.
[18] N. Broguiere, E. Cavalli, G.M. Salzmann, L.A. Applegate, M. Zenobi-Wong, Factor XIII cross-linked hyaluronan hydrogels for cartilage tissue engineering, ACS Biomater. Sci. Eng. 2 (12) (2016) 2176–2184.
[19] N. Broguiere, L. Isenmann, M. Zenobi-Wong, Novel enzymatically cross-linked hyaluronan hydrogels support the formation of 3D neuronal networks, Biomaterials 99 (2016) 47–55.
[20] C.P. Guimaraes et al., Site-specific C-terminal and internal loop labeling of proteins using sortase-mediated reactions, Nat. Protoc. 8 (9) (2013) 1787–1799.
[21] E. Cambria et al., Covalent modification of synthetic hydrogels with bioactive proteins via sortase-mediated ligation, Biomacromolecules 16 (8) (2015) 2316–2326.
[22] J. Valdez et al., On-demand dissolution of modular, synthetic extracellular matrix reveals local epithelial-stromal communication networks, Biomaterials 130 (2017) 90–103.
[23] M.R. Arkenberg, C.-C. Lin, Orthogonal enzymatic reactions for rapid crosslinking and dynamic tuning of PEG–peptide hydrogels, Biomater. Sci. 5 (11) (2017) 2231–2240.
[24] I. Chen, B.M. Dorr, D.R. Liu, A general strategy for the evolution of bond-forming enzymes using yeast display, Proc. Natl. Acad. Sci. 108 (28) (2011) 11399–11404.
[25] M.B. Gorbet, M.V. Sefton, Endotoxin: the uninvited guest, Biomaterials 26 (34) (2005) 6811–6817.
[26] J.M. Zuidema, C.J. Rivet, R.J. Gilbert, F.A. Morrison, A protocol for rheological characterization of hydrogels for tissue engineering strategies, J. Biomed. Mater. Res. B Appl. Biomater. 102 (5) (2014) 1063–1073.
[27] R.J. Gübeli et al., Pharmacologically tunable polyethylene-glycol-based cell growth substrate, Acta Biomater. 9 (9) (2013) 8272–8278.
[28] Y.K. Kim, E.Y. Chen, W.F. Liu, Biomolecular strategies to modulate the macrophage response to implanted materials, J. Mater. Chem. B 4 (9) (2016) 1600–1609.
[29] Z. Sheikh, P.J. Brooks, O. Barzilay, N. Fine, M. Glogauer, Macrophages, foreign body giant cells and their response to implantable biomaterials, Materials (Basel) 8 (9) (2015) 5671–5701.
[30] A. Rodriguez, S.R. MacEwan, H. Meyerson, J.T. Kirk, J.M. Anderson, The foreign body reaction in T-cell-deficient mice, J. Biomed. Mater. Res. A 90 (1) (2009) 106–113.
[31] C.M. O'Neill et al., Circulating levels of IL-1B+IL-6 cause ER stress and dysfunction in islets from prediabetic male mice, Endocrinology 154 (9) (2013) 3077–3088.
[32] A. Rodriguez, H. Meyerson, J.M. Anderson, Quantitative in vivo cytokine analysis at synthetic biomaterial implant sites, J. Biomed. Mater. Res. A 89 (1) (2009) 152–159.
[33] M.L. Bentley, H. Gaweska, J.M. Kielec, D.G. McCafferty, Engineering the substrate specificity of Staphylococcus aureus sortase A: the β6/β7 loop from SrtB confers npqtn recognition to SrtA, J. Biol. Chem. 282 (9) (2007) 6571–6581.
[34] M.P. Lutolf, N. Tirelli, S. Cerritelli, L. Cavalli, J. a Hubbell,, Systematic modulation of Michael-type reactivity of thiols through the use of charged amino acids, Bioconjug. Chem. 12 (6) (2001) 1051–1056.